Electron-impact ionization-excitation of the neon valence shell studied by high-resolution electron-momentum spectroscopy

J. M. Li,[1] Z. H. Luo,[1] X. L. Chen,[1] J. K. Deng,[1] and C. G. Ning[1,2,*]

[1]*Department of Physics, State Key Laboratory of Low-Dimensional Quantum Physics, Tsinghua University, Beijing 100084, China*

[2]*Collaborative Innovation Center of Quantum Matter, Beijing, China*

(Received 21 April 2015; published 2 September 2015)

We present experimental and theoretical results for electron-impact-induced ionization and excitation of the neon valence shell by using a highly sensitive and high-resolution $(e, 2e)$ spectrometer. The controversies in previous electron momentum spectroscopic results have been resolved. The satellites at 55.83 and 71.50 eV are mainly attributed to a ^2P manifold, and mixed up with some ^2S, not a pure ^2S as were assigned by the earlier electron-momentum spectroscopy. Our experimental momentum distribution for the satellite at 55.83 eV is consistent with that reported by Watanabe *et al.* [J. Electron Spectrosc. Relat. Phenom **142**, 325 (2005)], but not consistent with Samardzic *et al.*'s results [Phys. Rev. A **48**, 4390 (1993)]. The difference between the observed momentum distribution of the satellite at 55.83 eV and the calculations with the plane-wave impulse approximation suggests the need for further improvement of the theoretical methods.

DOI: 10.1103/PhysRevA.92.032701 PACS number(s): 34.80.Dp

I. INTRODUCTION

In high-resolution electron spectroscopy, some well-resolved additional weak satellites are often observed besides the main lines. These satellites are the results of ionization with simultaneous excitation. It is generally known as shakeup due to the electron-electron correlation in photoelectron spectroscopy [1]. Although the origin of satellites is clear, there are still many features which are not fully understood. The study of correlation satellites in the ionization spectra of rare gas atoms is still challenging from both theoretical and experimental sides [2–24]. The kinematically complete measurements of $(e, 2e)$ experiments can obtain angle-resolved differential cross sections and binding energy spectra simultaneously, which provides a more stringent test for the theoretical calculations [1,25]. Neon is one of the simplest targets for investigating the ionization-excitation process [13–20,26,27]. The first detailed electron momentum spectroscopic (EMS) study of neon satellites was carried out by Brunger and Weigold in 1992 [20] at an impact energy of 1500 eV, later extended by Samardzic *et al.* [28]. More recently, Watanabe *et al* reported $(e, 2e)$ experiments of neon at impact energies of 1250, 1450, and 1670 eV with a much higher statistic accuracy [29]. There are distinct differences between the experimental momentum distributions of the satellite at 55.83 eV reported by Samardzic *et al.* [28] and those by Watanabe *et al.* [29]. The possible reason for the inconsistency in these experimental results is the small cross section and insufficient energy resolution for discriminating the different final ion states. To resolve the issue, we present the $(e, 2e)$ satellites study using our high-resolution and high-sensitivity spectrometer. The measured momentum distributions are compared with the high-level symmetry-adapted-cluster (SAC) configuration-interaction (CI) theoretical calculations [30].

II. THEORETICAL AND EXPERIMENTAL METHODS

In a kinematically complete $(e, 2e)$ experiment, the momentum vectors of all free particles can be determined. Our $(e, 2e)$ spectrometer takes the noncoplanar symmetric geometry [31–33], as illustrated in Fig. 1. The incident electron (prepared with an energy E_i and a momentum $\vec{k}_i$) impacts on a neon atom and ionizes it. The two outgoing electrons are coincidently detected to determine their energies and momenta. Using the conservation of energy and momentum, we have

$$\vec{q} = \vec{k}_i - \vec{k}_f - \vec{k}_e, \tag{1}$$

$$E_b = E_i - E_f - E_e, \tag{2}$$

where $\vec{q}$ is the recoil momentum, E_b is the binding energy, E_f and $\vec{k}_f$ are the energy and momentum of the scattered projectile, and E_e and $\vec{k}_e$ those for the ejected electron. The two outgoing electrons have roughly equal energies ($E_f \approx E_e$) and equal polar angles ($q_f = q_e = 45^\circ$). The momentum of the electron before being knocked out can be obtained by measuring the relative azimuthal angle ϕ between the two outgoing electrons through

$$p = \left\{ [k_i - \sqrt{2}k_f]^2 + \left[\sqrt{2}k_f \sin\left(\frac{\phi}{2}\right) \right]^2 \right\}^{1/2}. \tag{3}$$

Under conditions of high impact energy and high momentum transfer, the differential cross section σ_{EMS} can be described with the plane wave impulse approximation (PWIA) [1] by

$$\sigma_{\mathrm{EMS}} \propto S_i^f \int d\Omega \left| \left\langle e^{-i\vec{p}\cdot\vec{r}} \Psi_f^{N-1} \middle| \Psi_i^N \right\rangle \right|^2, \tag{4}$$

where ${S_i}^f$ is the spectroscopic factor, $e^{-i\vec{p}\cdot\vec{r}}$ stands for the plane wave, ${\Psi_i}^N$ and ${\Psi_f}^{N-1}$ represent the wave functions of the neutral state and the ionized state of the target, respectively. N is the total electron number and $\int d\Omega$ represents the spherical average for the randomly oriented molecules in gas phase. The overlap integral $\langle \Psi_f^{N-1} | \Psi_i^N \rangle$ is called the Dyson orbital [31],

*ningcg@tsinghua.edu.cn

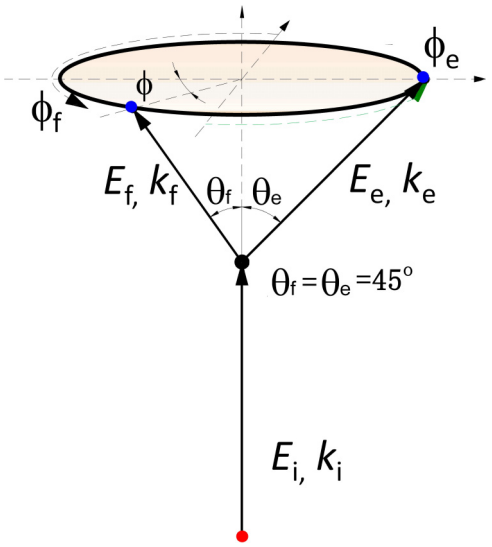

FIG. 1. (Color online) The non-coplanar symmetric geometry of $(e, 2e)$ experiment used in present work.

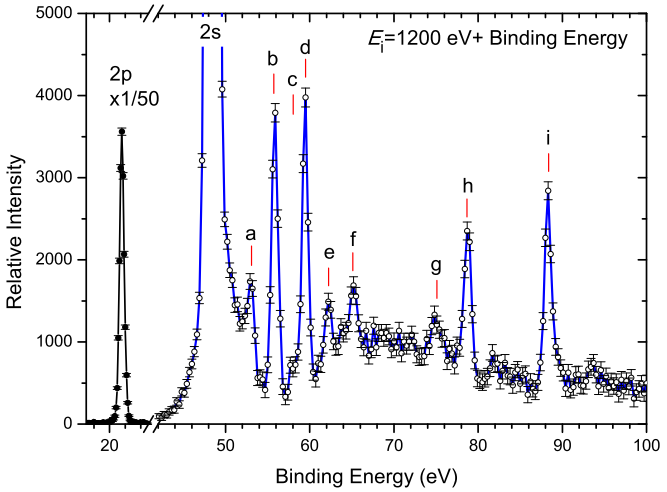

FIG. 2. (Color online) The binding energy spectrum of Ne obtained at the impact energies of 1200 eV plus binding energies. The intensity of peak 2p is scaled by a factor of 1/50.

which can be calculated using many-body theories, such as the configuration interaction or Green's function theory.

In the present work, the Dyson orbitals are generated using SAC-CI theory, which was originally developed by Nakatsuji [30]. Recently, we used the SAC-CI method to calculate momentum distributions of Dyson orbitals [34–38]. A home-compiled program, NEMS, is used to calculate the spherically averaged momentum distributions [39]. An augmented correlation-consistent polarized valence quadruple zeta (aug-cc-pVQZ) basis set is used in the present calculations [40]. The R operators up to sextuple are included. The active space includes 80 molecular orbitals. Perturbation selections are conducted to reduce the computation time. The threshold of the linked terms for the ground state is 1.0×10^{-6}, and the unlinked terms are included as the products of the linked terms whose single- and double- configuration-interaction (SDCI) coefficients are larger than 5.0×10^{-3}.

The energy resolution is 0.68 eV (the full width at half maximum, FWHM) at an impact energy of 1200 eV, which may deteriorate a little due to the very long running time, more than two months. The acceptance of the polar angle θ is $\pm 0.53°$, and the azimuthal angle ϕ resolution is $\pm 0.84°$ [31–33]. The purity of the neon gas sample is 99.999%.

III. RESULTS AND DISCUSSION

Figure 2 shows the binding energy spectrum of neon obtained at impact energies of 1200 eV plus binding energies. The spectrum is a summed result of the binding energy spectra of all azimuthal angles ϕ. Since the intensities of satellites are very weak, multiple scans were performed with the impact energy from 1242 to 1300 eV to accumulate enough counts. The neon $2p$ state was measured in a separated scan to check the momentum resolution of the spectrometer. It can be seen that there are eight well-resolved satellites (labeled as peaks a, b, d, e, f, g, h, and i) in Fig. 2. A noticeable shoulder at 58.02 eV is labeled as peak c according to the observation of the high-resolution photoelectron spectroscopy. The binding energies and assignment of these peaks are listed in Table I. To extract the experimental momentum distribution for each Ne^+ ion state, the spectra at a series of angles ϕ were fitted by 11 Gaussian peaks individually. The centers of those Gaussian peaks are the binding energies, as listed in Table I, and the widths (FWHM) of $2p$ and $2s$ are fixed as 0.7 and 0.9 eV; 1.4, 1.6, and 2.8 eV for peaks e, f, and g, respectively. The widths for peaks a, b, c, d, h, and i are all 0.8 eV. These broad widths of peaks e, f, and g are estimated for best fitting, which include the natural linewidths and the unresolved weak satellites. An intensity normalization procedure is applied to the experimental data for comparisons with the theoretical calculation. In Fig. 3, the experimental intensities of $2p$ and $2s$ states have been individually divided by the normalization factors for the best fitting with the calculations. Then the normalization factor for the $2s$ state is used to obtain the spectroscopic factors of the satellites. The value 0.869 predicted by the QDPT-CI calculations is used as the spectroscopic factor for the $2s$ state [44]. The theoretical momentum distributions have been convolved with the experimental momentum resolution by the Monte Carlo method [42]. The theoretical results are the spherically averaged momentum distributions of Dyson orbitals calculated by the SAC-CI method with PWIA. The calculated distribution is in excellent agreement with experimental results for the $2p$ state. For the $2s$ state, the PWIA calculation can well describe the experimental profile except for a small discrepancy in the high-momentum region (>1.3 a.u.), which is due to the distorted-wave effect [29].

Figure 4(a) shows the experimental momentum distribution for peak a (53.08 eV) in comparison with the calculations. It can be seen that it is a p-type distribution, which is consistent with the earlier assignment ^2P. Peak a is the result of ionization with simultaneous excitation: one $2p$ electron is ionized, and another $2p$ electron is excited to the $3p$ state. It is generally believed that the momentum distribution of a satellite is the same as that of its parent line. The experimental distribution agrees with the theoretical momentum distribution of the $2p$

TABLE I. Comparison of spectroscopic factors for ion states of neon. The error in the last significant figure is given in parentheses.

	E_b(eV)	Assignment	Present work	EMS[b]	EMS[c]	PES[d]	GF[e]	QDPT-CI[f]
$2s$	48.46	$2s^1 2p^6\,{}^2S$	0.869[a]	0.869	0.85(2)	0.869	0.874	0.869
a	53.08	$2s^2 2p^4({}^3P)3p\,{}^2P$	0.007(3)	0.004(1)	0.013(3)	0.007	0.003	0.004
b	55.83	$2s^2 2p^4({}^1D)3p\,{}^2P$	0.022(6)			0.020	0.018	0.012
		$2s^2 2p^4({}^1S)3s\,{}^2S$	0.004(2)		0.028(8)		0.017	0.011
c	58.02	$2p^4({}^3P)4p\,{}^2P$	0.005(3)			0.001	<0.001	0.003
d	59.49	$2s^2 2p^4({}^1D)3d\,{}^2S$	0.016(3)	0.011(2)	0.014(3)	0.008	0.013	0.008
		$2s^2 2p^4({}^1S)3p\,{}^2P$	0.004(2)	0.003(2)			0.011	0.002
e	62.19	$2s^2 2p^4({}^1D)4d\,{}^2S$	0.009(4)		0.025(6)	0.002	0.005	0.002
f	65.30	$2s^2 2p^4({}^1D)6d\,{}^2S$	0.010(4)			0.002	0.002	
g	75.10	$2s2p^5({}^3P)3s\,{}^2P$	0.007(3)			0.005	0.001	
		${}^2S$	0.003(2)		0.011(3)			
h	78.90	$2s^1 2p^5({}^1P)3p\,{}^2S$	0.015(3)	<0.015(2)	0.022(4)	0.011	0.009	
i	88.32	$2s^1 2p^5({}^1P)3p\,{}^2S$	0.018(3)	<0.019(3)	0.023(4)	0.028	0.025	

[a]The value of 0.869 is taken from the QDPT-CI calculations to determine spectroscopic factors of satellites.
[b]Reference [29].
[c]Reference [28].
[d]Reference [41]. The values of 0.928 and 0.869 are taken from the QDPT-CI calculations to convert the PES intensities to spectroscopic factors.
[e]Reference [42].
[f]Reference [43]. The work did not include the data for the binding energy higher than 65 eV.

state multiplied by a factor 0.007. Therefore, peak a is assigned as $2s^2 2p^4\ ({}^3P)3p\,{}^2P$ and its spectroscopic factor is measured as 0.007. In Fig. 4(b), the experimental distribution of peak c (58.02 eV) is compared with the theoretical momentum distribution of the $2p$ state multiplied by a factor 0.005.

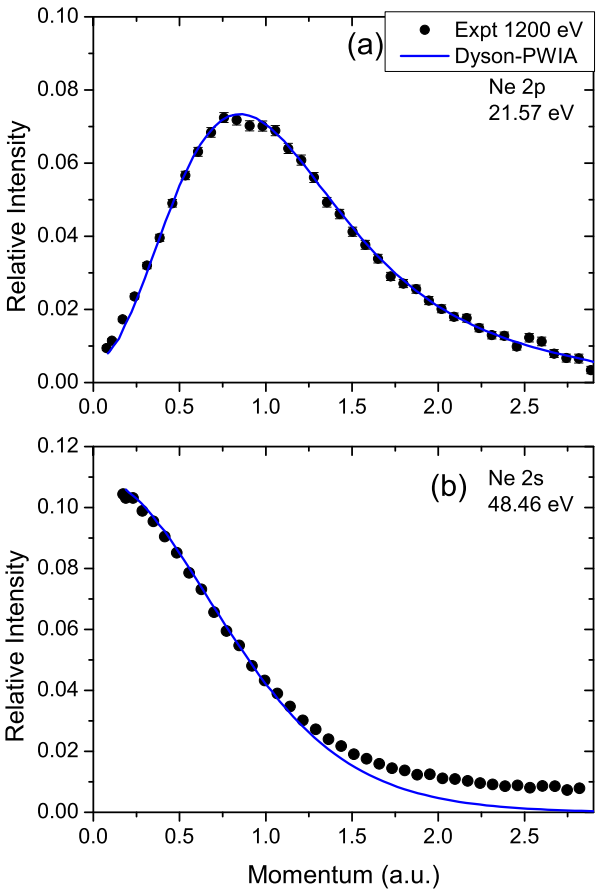

FIG. 3. (Color online) The experimental momentum distributions of Ne $2p$ and $2s$ states in comparison with the calculated distributions by SAC-CI method with the plane wave impulse approximation (solid curves).

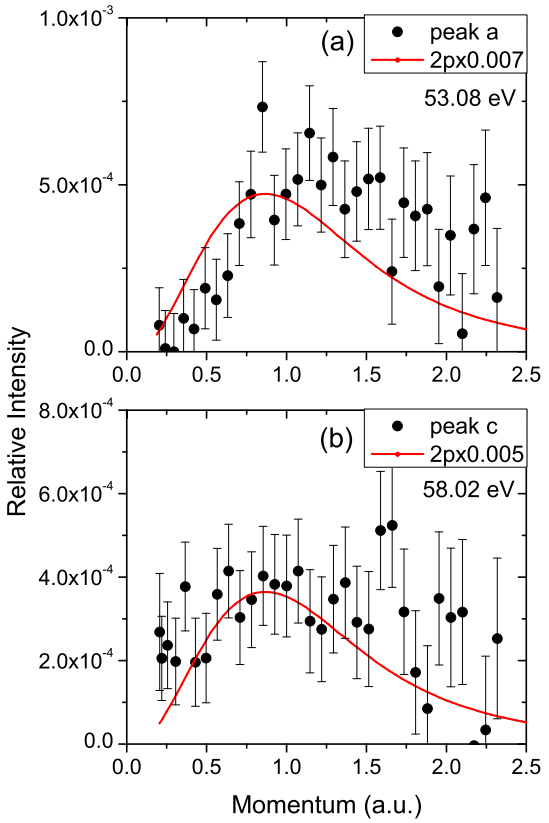

FIG. 4. (Color online) The experimental momentum distributions of peak a (53.08 eV) and peak c (58.02 eV) in comparison with the theoretical momentum distribution of $2p$ states multiplied by the spectroscopic factors, respectively.

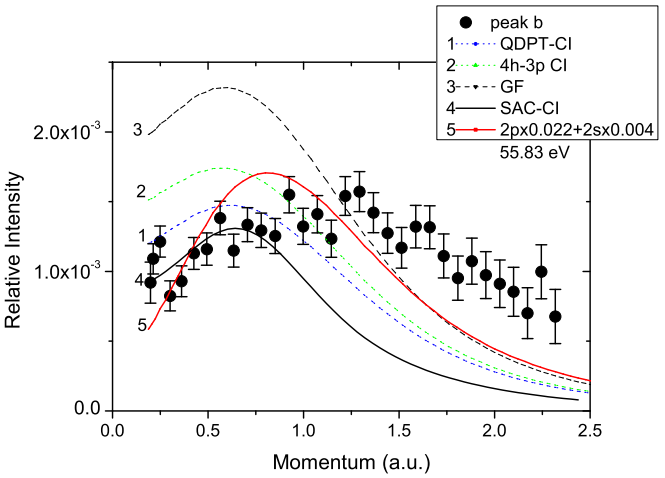

FIG. 5. (Color online) The experimental momentum distributions of peak b (55.83 eV) in comparison with various calculations.

Peak c is the result of the ionization of a $2p$ electron with a coincidental excitation from the $2p$ to $4p$ state. So it is assigned as $2p^4(^3P)4p\,^2P$ with a spectroscopic factor of 0.005.

Figure 5 shows the experimental momentum distribution for peak b (55.83 eV) in comparison with various theoretical calculations. At first sight, the profile of the experimental distribution is different from either an s type or a p type. An earlier EMS study assigned peak b to a pure ^2S manifold [28], while a more recent EMS study indicated that the experimental distribution cannot be simply described by a ^2S manifold [29]. Our experimental distribution agrees with the latter. The earlier theoretical calculations and photoemission spectroscopy (PES) study suggested that peak b was composed of two unresolved satellites. One is the $2s^22p^4\ (^1S)3s\,^2S$ ionic state, and the other is $2s^22p^4\ (^1D)3p\,^2P$. The theoretical calculations using quasidegenerate perturbation theory with configuration interaction (QDPT-CI) predicted that the spectroscopic factor of the ^2S ionic state is 0.0105, and 0.0119 for ^2P [44]. Therefore, the formula $2s \times 0.0105 + 2p \times 0.0119$ is used to reproduce the distribution (curve 1). It can be seen that curve 1 drops too fast, not in agreement with the experimental distribution. Curve 2 is generated by the formula $2s \times 0.0134 + 2p \times 0.0127$ according to calculations using the four-hole-three-particle configuration interaction (4h-3p CI) [45]. It cannot well describe the experimental results either. Curve 3 is generated using $2s \times 0.0175 + 2p \times 0.0174$, which is based on the results predicted by the Green function (GF) [46], and significantly overestimated the experimental intensity in the low-momentum region. The results presented here are consistent with the work by Watanabe *et al.* They suggest that this may be due to breakdown of the target Hartree-Fock approximation. Indeed, the EMS studies for satellites of He and H_2O have shown that the electron momentum distribution of a satellite can be different from its parent line in certain cases [2,39]. Therefore, the high-level SAC-CI theory was directly used to calculate the momentum distributions of Dyson orbitals related to peak b using Eq. (4). Two Dyson orbitals, the ^2P manifold with a spectroscopic factor 0.0123 and the ^2S manifold with a spectroscopic factor 0.0116, were obtained. Curve 4 shows the sum of their momentum distributions.

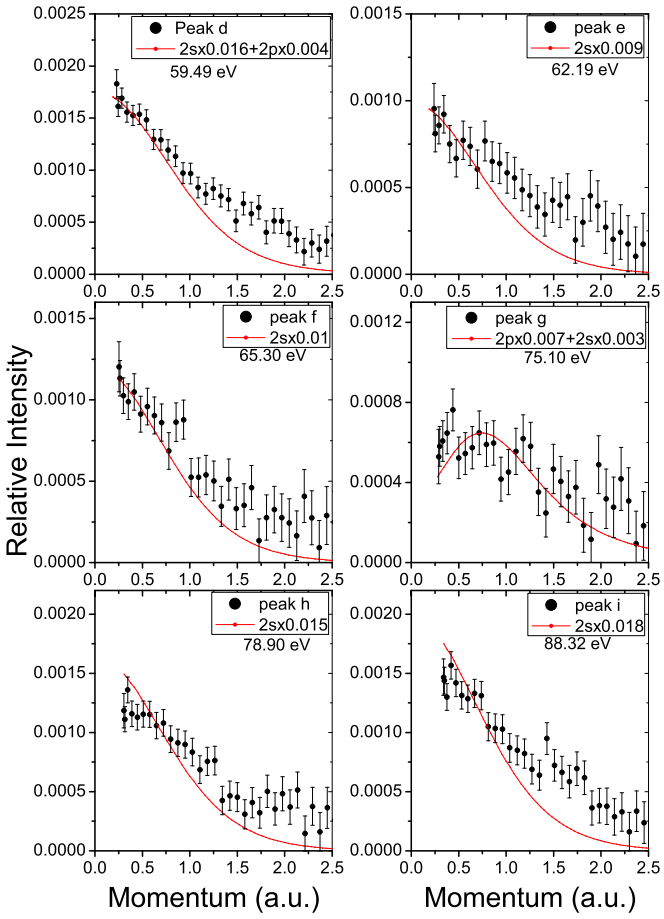

FIG. 6. (Color online) The experimental momentum distributions of peaks d (59.49 eV), e (62.19 eV), f (65.30 eV), g (75.10 eV), h (78.90 eV), i (88.32 eV) in comparison with the theoretical momentum distribution of $2s$ and $2p$ states multiplied by the spectroscopic factors, respectively.

It is in agreement with the experimental distribution in the low-momentum region (<0.8 a.u.). However, a significant discrepancy still exists in the high-momentum region. The calculated intensity decreases too fast as the momentum increases. The best-fitting curve 5 is plotted to estimate the spectroscopic factors, which is generated by using the formula $2p \times 0.022 + 2s \times 0.004$. Thus, the spectroscopic factor for the ^2P manifold is estimated as 0.022, and 0.004 for the ^2S manifold. It should be noted that the estimation may have significant errors because the agreement between PWIA calculations and the experimental distribution is not excellent.

Figure 6 shows the experimental momentum distributions for peaks d, e, f, g, h, and i. As shown in the figure, the experimental momentum distribution of peak d (59.49 eV) is dominantly s type. The GF and QDPT-CI calculations indicated that peak d is composed of two unresolved satellites. One is $2s^22p^4\ (^1D)3d\,^2S$, and the other is $2s^22p^4\ (^1S)3p\,^2P$. Therefore, the theoretical momentum distributions of $2p$ and $2s$ states are combined to reproduce the experimental distribution of peak d. The best fitting is $2s \times 0.016 + 2p \times 0.004$. As a result, the spectroscopic factor for the ^2S manifold is estimated as 0.016, and 0.004 for the ^2P manifold. This is consistent with the results of Ref. [29] within error bars. The

experimental momentum distribution of peak e (62.19 eV) is s type, which is consistent with the assignment $2s^2 2p^4 (^1D)4d\,^2S$ ionic state by GF theory [46]. The experimental spectroscopic factor is measured as 0.009. The value 0.025 reported by earlier EMS [28] overestimated its spectroscopic factor. Similarly, the peak f (65.30 eV) is assigned as $2s^2 2p^4 (^1D)6d\,^2S$ with a spectroscopic factor 0.010. The measured momentum distribution of peak g (75.10 eV) is different from that of peak f, which cannot be well described by either by a ^2S manifold or a ^2P manifold alone. A best-fitting result is $2p \times 0.007 + 2s \times 0.003$. Its main contribution is the ^2P manifold, which is consistent with GF theory and PES study results, both assigning it as $2s2p^5(^3P)3s\,^2P$ ionic state. The small contribution from the ^2S manifold (0.003) may be due to the influence of the continuum background, as seen in Fig. 2. The double-ionization limit of Ne, the lowest energy for producing the Ne^{2+} ion, is 62.52 eV [47]. The earlier EMS study [28] assigning peak g as the ^2S manifold with a spectroscopic factor 0.011 is not consistent with our observation. Both peaks h (78.90 eV) and i (88.32 eV) are s type. The spectroscopic factors are measured as 0.015 and 0.018, respectively, which are consistent with the earlier EMS studies [28,29]. It should be noted that the $(e, 2e)$ experimental technique cannot discriminate the double ionization from the single ionization if both can happen. Therefore, the measured spectroscopic factors of the peaks e, f, g, h, and i may have a systemic error due to the influence of the double ionization, especially for the weak peaks e, f,and g. The contribution of the $2S$ manifold for these peaks may be overestimated because the experimental momentum distribution of the continuum background looks s type. Moreover, the high-level GF calculation [46] predicted 42 satellites in total. Only nine satellites with higher intensities clearly showed up in our experiment. Therefore, the observed momentum distributions may be mixed up partly with those unresolved weak satellites. In Table I, spectroscopic factors of Ne satellites from this study are compared with those of the earlier studies in detail. In general, this work agrees with the high-level theoretical predictions for symmetries and spectroscopic factors of the neon satellites.

Why cannot the theoretical calculations describe the experimental distribution of peak b (55.83 eV) in Fig. 5? Peak b is a rather strong peak and its binding energy is below the double-ionization limit. The influence of other states and the background to peak b can be ruled out. Our observed momentum distribution is almost the same as that reported by Watanabe *et al.* [29]. Therefore, the discrepancy we observed must be due to some real physical mechanisms that are not included in the PWIA calculations. The possibility for the discrepancy due to the electron correlation in the initial neutral state and the final ionized state should be small because the SAC-CI calculation, which has considered the electron correlation at a very high level, still cannot reproduce the experimental momentum distribution. One possible source for the discrepancy is the collision dynamics. All the theoretical momentum distributions in the present work were calculated with the PWIA. Our recent work on ionization-excitation of He has shown that the post-collision Coulomb interaction (PCI) can remarkably change the momentum distributions of satellites $n = 2,3,4,5$ for He^+ [2]. The four-body distorted wave calculation, which has taken into account PCI between the scattered projectile and the ejected electron, can well describe the experimental momentum distributions. It is interesting to note that experimental intensity for satellites of He in the high-momentum region is also higher than that of the calculation without PCI, which is similar to the present observation for peak b. The importance of PCI in the electron-impact ionization process has been clearly demonstrated by recent low-energy $(e, 2e)$ work on Ne $2p$ [41]. An excellent agreement was found between the experimental data and the calculations based on the three-body distorted-wave approach and the B-spline R-matrix with pseudostates approach. Such a sophisticated calculation is eagerly awaited for peak b to verify or deny the PCI effects on the momentum distributions.

IV. CONCLUSIONS

High-resolution EMS measurements at 1200 eV have been conducted for the ionization-excitation of the Ne valence shell. It was found that the main contributions to the satellites at 55.83 and 71.50 eV are the $2P$ manifold, and mixed up with some $2S$, not a pure $2S$ as assigned by the earlier electron momentum spectroscopy. The theoretical calculations with the plane-wave impulse approximation cannot well describe the experimental momentum distribution of peak b (55.83 eV). At the current stage, the physical mechanism behind the discrepancy is still not clear; it needs further high-level theoretical calculations to explain the observed distributions.

ACKNOWLEDGMENTS

This work is supported by the National Natural Science Foundation of China (NSFC) (Grants No. 11174175 and No. 91336104) and the Ministry of Science and Technology of China (MOST) (Grant No. 2013CB922004) of the National Key Basic Research Program of China.

[1] E. Weigold and I. E. McCarthy, *Electron Momentum Spectroscopy* (Kulwer Academic, New York, 1999).
[2] X. L. Chen, A. L. Harris, J. M. Li, T. P. Esposito, J. K. Deng, and C. G. Ning, Phys. Rev. A **89**, 062713 (2014).
[3] O. Zatsarinny and K. Bartschat, J. Phys. B **47**, 061001 (2014).
[4] X. Ren, I. Bray, D. V. Fursa, J. Colgan, M. S. Pindzola, T. Pflüger, A. Senftleben, S. Xu, A. Dorn, and J. Ullrich, Phys. Rev. A **83**, 052711 (2011).
[5] D. A. Horner, C. W. McCurdy, and T. N. Rescigno, Phys. Rev. A **71**, 010701 (2005).
[6] C. D. Cappello, A. C. Roy, X. G. Ren, and R. Dey, Nucl. Instrum. Methods Phys. Res. B **266**, 570 (2008).
[7] G. Sakhelashvili, A. Dorn, C. Höhr, J. Ullrich, A. S. Kheifets, J. Lower, and K. Bartschat, Phys. Rev. Lett. **95**, 033201 (2005).
[8] X. G. Ren, C. G. Ning, J. K. Deng, G. L. Su, S. F. Zhang, Y. R. Huang, and G. Q. Li, Phys. Rev. A **72**, 042718 (2005).

[9] N. Watanabe, M. Takahashi, Y. Udagawa, K. A. Kouzakov, and Y. V. Popov, Phys. Rev. A **75**, 052701 (2007).
[10] S. Bellm, J. Lower, E. Weigold, I. Bray, D. V. Fursa, K. Bartschat, A. L. Harris, and D. H. Madison, Phys. Rev. A **78**, 032710 (2008).
[11] S. Bellm, J. Lower, K. Bartschat, X. Guan, D.Weflen, M. Foster, A. L. Harris, and D. H. Madison, Phys. Rev. A **75**, 042704 (2007).
[12] P.J. Marchalant, B. Rouvellou, J. Rasch, S. Rioual, C. T. Whelan, A. Pochat, D. H. Madison, and H. R. Walters, J. Phys. B **33**, L749 (2000).
[13] U. Becker, R. Wehlitz, O. Hemmers, B. Langer, and A. Mentzel, Phys. Rev. Lett. **63**, 1054 (1989).
[14] A. D. O. Bawagan, B. J. Olsson, K. H. Tan, J. M. Chen, and G. M. Bancroft, Chem. Phys. Lett. **179**, 344 (1991).
[15] M. O. Krause, S. B. Whitfield, C. D. Caldwell, J. Z. Wu, P. van der Meulen, C. A. de Lange, and R. W. C. Hansen, J. Electron Spectrosc. Relat. Phenom. **58**, 79 (1992).
[16] M. Pahler, C. D. Caldwell, S. J. Schaphorst, and M. D. Krause, J. Phys. B **26**, 1617 (1993).
[17] P. Bolognesi, L. Avaldi, D. R. Cooper, M. Coreno, R. Camilloni, and G. C. King, J. Phys. B **35**, 2927 (2002).
[18] A. J. Dixon, I. E. McCarthy, C. J. Noble, and E. Weigold, Phys. Rev. A **17**, 597 (1978).
[19] K. T. Leung and C. E. Brion, Chem. Phys. **82**, 87 (1983).
[20] M. J. Brunger and E. Weigold, J. Phys. B **25**, 481 (1992).
[21] I. E. McCarthy, R. Pascual, P. Storer, and E. Weigold, Phys. Rev. A **40**, 3041 (1989).
[22] M. J. Brunger, I. E. McCarthy, and E. Weigold, Phys. Rev. A **59**, 1245 (1999).
[23] R. Nicholson, S. W. Braidwood, I. E. McCarthy, E. Weigold, and M. J. Brunger, Phys. Rev. A **53**, 4205 (1996).
[24] S. Braidwood, M. Brunger, and Erich Weigold, Phys. Rev. A **47**, 2927 (1993).
[25] T. Pfluger, O. Zatsarinny, K. Bartschat, A. Senftleben, X. G. Ren, J. Ullrich, and A. Dorn, Phys. Rev. Lett. **110**, 153202 (2013).
[26] M. A. Stevenson, L. R. Hargreaves, B. Lohmann, I. Bray, D.V. Fursa, K. Bartschat, and A. Kheifets, Phys. Rev. A **79**, 012709 (2009).
[27] C. P. Ballance, J. A. Ludlow, M. S. Pindzola, and S. D. Loch, J. Phys. B **42**, 175202 (2009).
[28] O. Samardzic, S. W. Braidwood, E. Weigold, and M. J. Brunger, Phys. Rev. A **48**, 4390 (1993).
[29] N. Watanabe, Y. Khajuria, M. Takahashi, and Y. Udagawa, J. Electron Spectrosc. Relat. Phenom **142**, 325 (2005).
[30] H. Nakatsuji, Chem. Phys. Lett. **59**, 362 (1978).
[31] C. G. Ning, S. F. Zhang, J. K. Deng, K. Liu, Y. R. Huang, and Z. H. Luo, Chin. Phys. B **17**, 1729 (2008).
[32] C. G. Ning, J. K. Deng, G. L. Su, H. Zhou, and X. G. Ren, Rev. Sci. Instrum. **75**, 3062 (2004).
[33] X. G. Ren, C. G. Ning, J. K. Deng, S. F. Zhang, G. L. Su, F. Huang, and G. Q. Li, Rev. Sci. Instrum. **76**, 063103 (2005).
[34] Y. Liu, L. F. Cheung, and C. G. Ning, Chin. Phys. B **23**, 063403 (2014).
[35] Y. R. Miao, C. G. Ning, and J. K. Deng, Phys. Rev. A **83**, 062706 (2011).
[36] Y. R. Miao, C. G. Ning, K. Liu, and J. K. Deng, J. Chem. Phys. **134**, 204304 (2011).
[37] J. S. Zhu, J. K. Deng, and C. G. Ning, Phys. Rev. A **85**, 052714 (2012).
[38] Y. R. Miao, J. K. Deng, and C. G. Ning, J. Chem. Phys. **136**, 124302 (2012).
[39] C. G. Ning, B. Hajgato, Y. R. Huang, S. F. Zhang, K. Liu, Z. H. Luo, S. Knippenberg, J. K. Deng, and M. S. Deleuze, Chem. Phys. **343**, 19 (2008).
[40] T. J. Dunning, Jr., J. Chem. Phys. **90**, 1007 (1989).
[41] X. G. Ren, S. Amami, O. Zatsarinny, T. Pflüger, M. Weyland, W. Y. Baek, H. Rabus, K. Bartschat, D. Madison, and A. Dorn, Phys. Rev. A **91**, 032707 (2015).
[42] P. Duffy, M. E. Casida, C. E. Brion, and D. P. Chong, Chem. Phys. **159**, 347 (1992).
[43] A. Kikas, S. J. Osborne, A. Ausmees, S. Svensson, O. P. Sairanen and S. Aksela, J. Electron Spectrosc. Relat. Phenom. **77**, 241 (1996).
[44] G. Fronzoni and P. Decleva, Chem. Phys. **220**, 15 (1997).
[45] P. Decleva, G. De Alti, G. Fronzoni, and A. Lisini, J. Phys. B **23**, 3777 (1990).
[46] A. S. Kheifets, J. Phys. B **28**, 3791 (1995).
[47] R. I. Hall, K. Ellis, A. McConkey, G. Dawber, L. Avaldi, M. A. MacDonald, and G. C. King, J. Phys. B **25**, 377 (1992).